# EXPLORATION OF CIGAS ALLOY SYSTEM FOR THIN-FILM PHOTOVOLTAICS ON NOVEL LIGHTWEIGHT AND FLEXIBLE SUBSTRATES

**Lawrence M. Woods, Ajay Kalla, and Rosine Ribelin**
ITN Energy Systems Inc., Littleton, CO

## INTRODUCTION

Thin-film photovoltaics (TFPV) on lightweight and flexible substrates offer the potential for very high solar array specific power (W/kg). ITN Energy Systems, Inc. (ITN) is developing flexible TFPV blanket technology that has potential for specific power greater than 2000 W/kg (including space coatings) that could result in solar array specific power between 150 and 500 W/kg, depending on array size, when mated with mechanical support structures specifically designed to take advantage of the lightweight and flexible substrates.(1) This level of specific power would far exceed the current state of the art for spacecraft PV power generation, and meet the needs for future spacecraft missions.(2) Furthermore the high specific power would also enable unmanned aircraft applications and balloon or high-altitude airship (HAA) applications, in addition to modular and quick deploying tents for surface assets or lunar base power, as a result of the high power density ($W/m^2$) and ability to be integrated into the balloon, HAA or tent fabric. ITN plans to achieve the high specific power by developing single-junction and two-terminal monolithic tandem-junction PV cells using thin-films of high-efficiency and radiation resistant $CuInSe_2$ (CIS) partnered with bandgap-tunable CIS-alloys with Ga (CIGS) or Al (CIAS) on novel lightweight and flexible substrates. Of the various thin-film technologies, single-junction and radiation resistant CIS and associated alloys with gallium, aluminum and sulfur have achieved the highest levels of TFPV device performance, with the best efficiency reaching 19.5% under AM1.5 illumination conditions and on thick glass substrates.(3) Thus, it is anticipated that single- and tandem-junction devices with flexible substrates and based on CIS and related alloys will achieve the highest levels of thin-film space and HAA solar array performance.

ITN is currently developing single-junction TFPV using wide-bandgap $CuInGaAlSe_2$ (CIGAS) on semi-transparent back contacts and novel silicone substrates to achieve better single-junction cell performance than low-bandgap CIGS on thin metal foils. A cross-sectional illustration of this configuration is given in Figure 1. Wide-bandgap TFPV devices offer several performance advantages over standard low-bandgap CIGS devices, including: better suited for high voltage applications; lower resistive losses for cells and

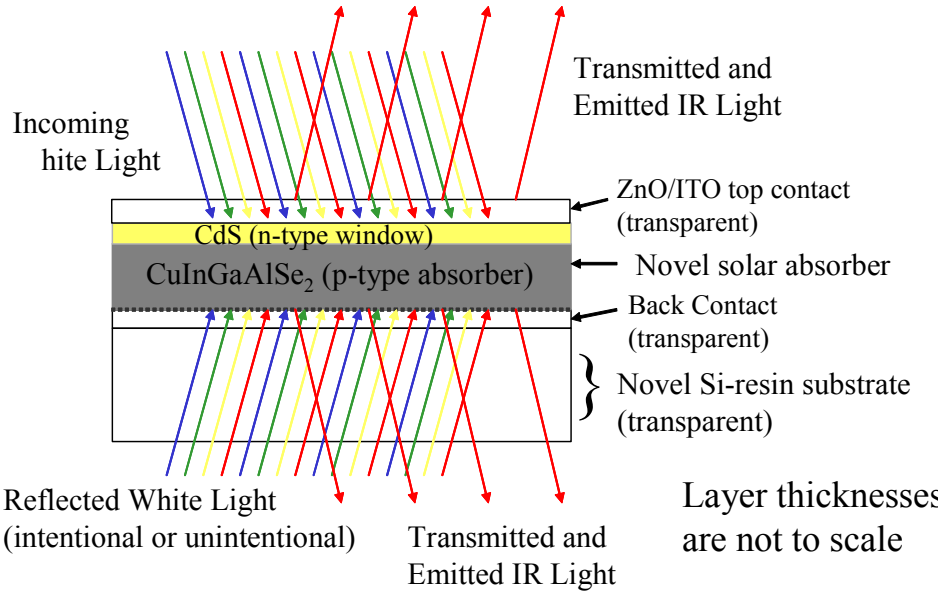


**Figure 1 – Cross-sectional (not to scale) illustration of wide-bandgap CIGAS device with semi-transparent back contacts and**

modules; transmits more unused infra-red light for lower temperature operation; and produces higher power during high-temperature applications due to lower temperature coefficients. A wide-bandgap CIGAS single-junction device with semi-transparent back contacts would enable bifacial power generation when combined with a transparent substrate, and could be the predecessor to a top cell with transparent back contact and interconnect components in a monolithic tandem-junction device.

The novel silicone substrates under development at ITN offer several performance advantages over thin metal foil and polyimide lightweight and flexible substrates. The silicone advantages include: higher temperature capability than polyimide, capable of monolithic integration and lighter weight compared to thin metal foils. The higher temperature capability is enabling for higher efficiency CIGS devices. Furthermore, the potential optical transparency of the silicone enables bifacial light collection and better IR transmittance than polyimide or thin metal foil substrates. To date, ITN has fabricated over 13% efficient (AM1.5) low-bandgap CIGS devices on the experimental silicone substrates, matching that of companion devices on glass substrates.

## NOVEL WIDE-BANDGAP CIGAS ALLOY THIN-FILM DEVICES

ITN has been developing wide-bandgap CIAS for several years using a large-area, production-like, co-evaporation deposition system. The original impetus for using $CuIn_{1-x}Al_xSe_2$ (CIAS) was the drop in efficiency observed with cells made from $CuIn_{1-x}Ga_xSe_2$ (CIGS) when x exceeds 0.3, thought to be due to Ga related defects accompanying high levels of Ga alloying. (4,5) The potential advantage of CIAS is that, for a given wide bandgap, much less Al alloying is needed compared to alloying with Ga,(6) and thus potentially avoiding defect formation associated with higher alloy (Ga or Al) content materials. R&D CIAS devices with efficiencies over 10% have been fabricated with bandgap ≈ 1.5 eV (x = 0.5).(7) However, despite the lower degree of alloying for a given bandgap, the wide-bandgap CIAS device performance seems to be no better than the wide-bandgap CIGS device performance. Nonetheless, there are distinct differences between the wide-bandgap CIGS and CIAS materials, which led us to believe that the solar absorber could be optimized using both Ga and Al to form CIGAS. Brief rational is discussed as follows:

1) Optimized free carrier density in the device junction region. An increasing depletion width (lower free carrier density) was measured with increasing Al content in CIS and correlated to lower voltage devices.(8) On the other hand, when adding Ga in CIS the opposite trend is measured as the free carrier density increases with increasing Ga content.(9,10) Thus using both Ga and Al can potentially enable the maintenance of optimal free carrier densities while increasing the bandgap to the desired energy.

2) Diminish the possibility of exceeding specific deep defect concentrations related to too much Ga or too much Al. CIGS device modeling suggests that a single dominant deep defect level can dictate the device performance. While the total defect concentration (integrated across the bandgap) may not be reduced, the peak defect concentration of a single dominant deep defect at a specific energy level, related to Ga or Al, could be reduced. (11)

3) Reduce level of undesirable phases at a given bandgap. Spinodal decomposition phenomena is predicted to be worse in CIAS than CIGS due to aluminum's smaller atomic size (higher diffusivity) and higher affinity for oxygen,(12) thus increasing the likelihood of localized high Al containing areas or Al-related defects and Al oxide phases. Confirmation of aluminum's affinity for oxygen is demonstrated in characterization work on the $CuAlSe_2$ endpoint ternary, which showed that this material had a high concentration of both aluminum not in the $CuAlSe_2$ matrix and oxygen.(13)

4) Enable heterointerface band offset optimization. Theoretically, the addition of Ga in CIS widens the bandgap by increasing the conduction band (CB) energy and leaving the valence band (VB) energy relatively unchanged.(14) On the other hand the addition of Al to CIS widens the bandgap by increasing the CB energy *and* decreasing the VB energy (16% of bandgap change). Thus, adding Al to CIGS would better maintain a small CB spike at the CdS/CIGAS heterointerface for the 1.45 eV targeted bandgap, and modeled to be beneficial to device performance.(15) Conversely, adding Ga to CIAS could decrease the back contact Schottky barrier height by reducing the VB band offset to the back contact, and consequently decrease the series resistance.

5) Enable smart solar absorber layer design for devices. Varying both Ga and Al as a function of film depth opens the possibility of maintaining a desired bandgap while varying and optimizing the layer material properties as a function of depth. For example, one level of Ga and Al alloying may be optimum toward the front of the device while a second level of Al or Ga alloying may be better at the back of the device. A similar tactic of material and bandgap tailoring as a function of depth is used in the highest efficiency low-bandgap CIGS solar cell absorbers, with the variation in Ga and sulfur (surface treatment).

This paper discusses the performance, and testing of the novel wide-bandgap single-junction CIGAS device on both glass substrates and the novel silicone substrates, and with both transparent back contacts and opaque Mo control back contacts.

## EXPERIMENT

Using the large-area and moving substrate co-evaporation deposition system at ITN, and previously configured for CIAS, ITN researchers adapted the chamber for CIGAS depositions with the added Ga source and for simultaneous delivery of the CIGAS elements. This yielded roughly constant Al and Ga content through the film (i.e. no bandgap grading). The Al to group III ratio or Al/(In+Ga+Al) or Al/III, and the Ga to group III ratio or Ga/III were systematically varied for each deposition to achieve a wide range of compositions and bandgaps. Furthermore, these ratios varied across each substrate as an intentional result of the source set-up. The target bandgap was varied but typically within the range of 1.45 eV $\pm$ 0.15 eV, the theoretical optimum for single-junction devices in the air mass zero solar spectrum. Several new CIAS (no Ga) devices were fabricated as control devices for later comparison with the CIGAS devices. The Cu/III ratio was targeted in a narrow range ($\pm$ 0.1) that gave the best devices. The CIGAS compositions were measured in a scanning electron microscope (SEM) by energy dispersive spectroscopy (EDS) at five points across each 5.5" wide sample. The substrate heater temperature was 575ºC during all the CIGAS depositions, including those on the novel silicone substrate.

Two types of back contacts were fabricated for the CIGAS devices, one type with standard molybdenum (Mo) back contacts, and a second type with transparent back contacts (TBCs). Most of the devices were fabricated on TBCs and on soda-lime glass substrates as these back-contacts and substrates were more readily available at ITN. When target compositions were obtained then the Mo back contacts and more novel silicone substrates were used.

To finish the devices the CIAS and CIGAS samples received CdS deposited by chemical bath deposition (CBD), ZnO/ITO top contact layers by sputter deposition, and e-beamed Al grids. Devices were patterned for 1 $cm^2$ sized devices.

## DEVICE RESULTS AND DISCUSSION

After fabrication, CIGAS TFPV devices were tested for device performance using current-voltage measurements (IV) under a solar simulator using AM1.5 illumination. If devices performed well, then they were also tested for quantum efficiency (QE) to estimate the bandgap by using the long wavelength (nm) value where the QE is about 1/3 of the maximum QE. Typically this method has closely correlated with the long wavelength inflection point in the QE and also with the empirical bandgap value based on the EDS determined Al/III ratio for CIAS devices. The device efficiency and open circuit voltage (Voc) as a function of bandgap for the better devices are shown in Figure 2 for the devices with Mo back contacts on glass. All CIAS samples needed a post fabrication air anneal to maximize their performance. This seemed to be less necessary as the Ga content was increased in the devices. Only the maximum performance is shown.

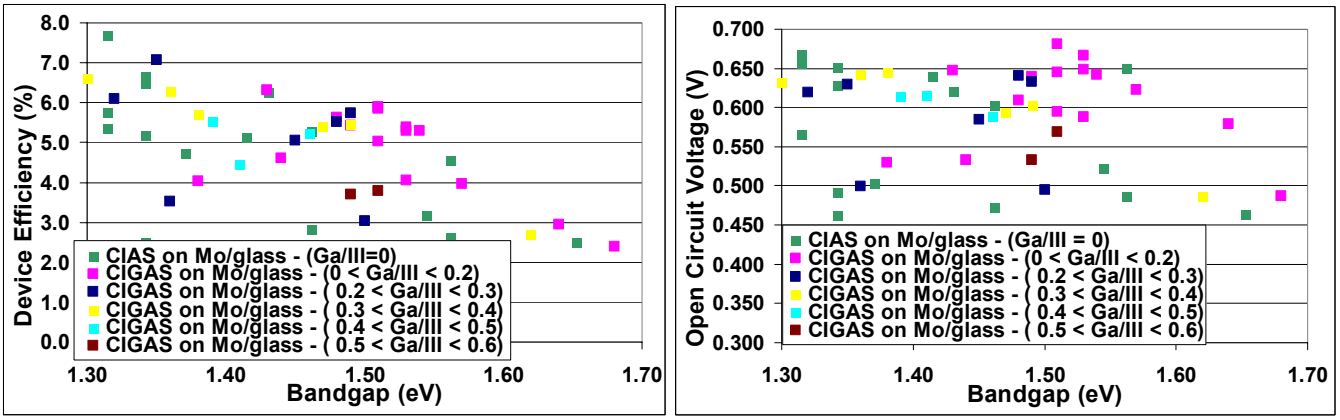


**Figure 2 – Recent CIAS and CIGAS device efficiency (left) and open circuit voltage or Voc (right) versus bandgap and Ga content (Al content). Mo back contact device results shown only.**

In general, over the entire bandgap range plotted, the efficiency and open-circuit voltage (Figure 2) plots indicate that the CIGAS devices on Mo back contacts appear to be roughly equivalent to that of the CIAS (no Ga) devices, and follow the same decrease in efficiency with increasing bandgap, with the voltages all limited to about 650 mV in the bandgap range of 1.35 to 1.55 eV. Looking more closely at the data as a function of Ga content in the bandgap range of 1.4 eV to 1.55 eV, the devices with low Ga content (pink and dark blue dots) have given the best results to date, suggesting that an optimum Ga content may exist in this bandgap range. A similar set of plots for the CIGAS devices on the transparent back contacts (TBCs) and glass substrates are shown in Figure 3.

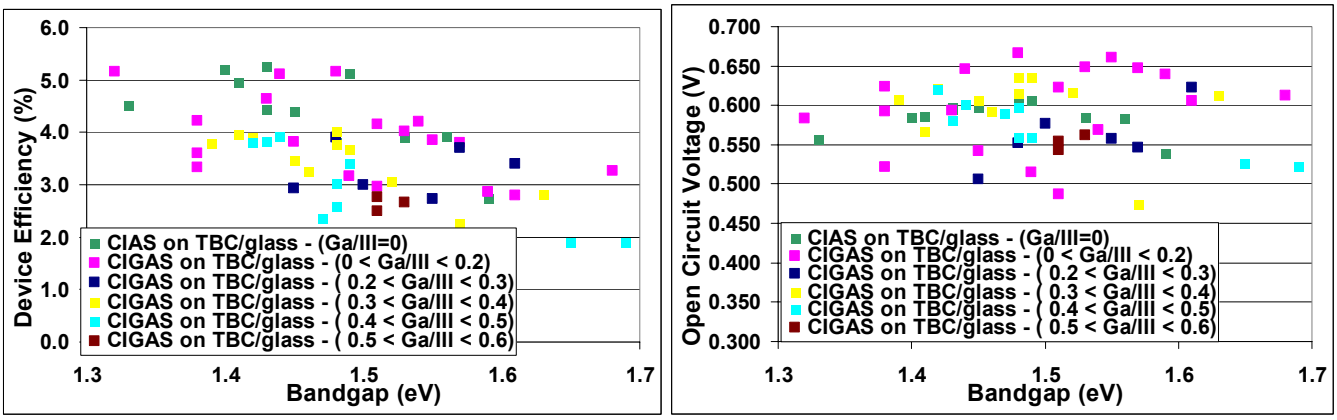


**Figure 3 – Recent CIAS and CIGAS device efficiency (left) and open circuit voltage or Voc (right) versus bandgap and Ga content (Al content). Transparent back contact (TBC) device results shown only.**

For these CIGAS devices, the low Ga (pink dots) show similar efficiencies to the CIAS controls up to a bandgap of about 1.55 eV, while higher amounts of Ga (yellow and light blue dots) seem to be detrimental to the performance. The plot of Voc versus bandgap reveals that the best (highest valued ones) CIGAS devices with low Ga (pink dots) have approximately 10% higher Voc than the best CIAS (no Ga) devices. Thus these results also indicate that a performance benefit may be realized with optimization of the Ga content in the CIGAS devices on TBCs.

The devices with Mo back contacts currently perform better than the TBCs as they have lower series resistance than the TBCs and do not block beneficial sodium from diffusing into the solar absorber during deposition. The availability of sodium and its benefits may also be equalizing the performance of the CIGAS devices on Mo back contacts.

Further characterization was performed on the best devices with Mo back contact on glass, and in a narrow bandgap range of 1.45 eV to 1.48 eV. Devices in this bandgap range had about the same performance (Eff. ≅ 5.0% - 5.6%), despite the wide-variation in Ga and Al composition. Figure 4 shows the light IV curves and QE's from the devices tested and the inset table shows the solar cell parameters from the light IV, bandgap from the QE, Al/III ratio and Ga/III ratio from the EDS, and the measured zero bias depletion width from capacitance voltage (CV) measurements.

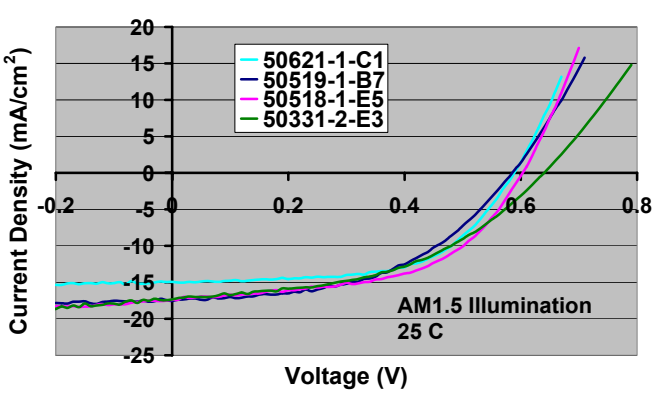


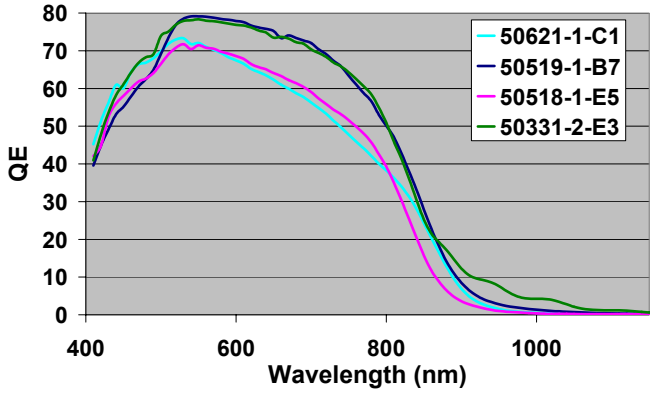


| Device ID | Eff. (%) | Voc (V) | Jsc (mA/cm$^2$) | FF | Diode Factor | Bandgap* | Al/III** | Ga/III** | Depletion Width*** (μm) |
|---|---|---|---|---|---|---|---|---|---|
| 50621-1-C1 | 5.23 | 0.589 | 14.93 | 0.60 | 3.2 | 1.46 | 0.16 | 0.49 | 0.19 |
| 50519-1-B7 | 5.04 | 0.585 | 17.57 | 0.49 | 4.9 | 1.45 | 0.23 | 0.25 | 0.27 |
| 50518-1-E5 | 5.63 | 0.603 | 17.40 | 0.54 | 3.6 | 1.48 | 0.35 | 0.17 | 0.23 |
| 50331-2-E3 | 5.14 | 0.64 | 17.33 | 0.46 | 4.7 | 1.46 | 0.43 | 0 | 0.25 |

* From QE, ** From EDS, *** From CV

**Figure 4 – Light IV curves (left) and QE's (right) from some of the best CIGAS devices with a bandgap in the narrow range of 1.45 – 1.48 eV, and as a function of Ga content (or Al content, see table).**

The light IV's and QE's do not indicate a trend with increasing Ga content (decreasing Al content), but it is noted that the devices with the higher fill factor and lower diode factors, correlated with the QE's showing more wavelength dependent collection with reduced collection at longer wavelengths. The zero bias depletion width was similar for all the devices (dielectric constant assumed to be the same for all samples) and thus indicates that they all have similar net free carrier densities in the junction region. The devices were characterized for defect density and energy level by admittance spectroscopy (AS) using the method of Walter *et al*.(16) For this method, capacitance versus frequency measurements were performed in the dark from 500 to 250 kHz using a Hewlett-Packard 4192A LF impedance analyzer, at zero bias and at a modulation voltage of 0.1 V. The temperatures ranged from 180 K to room temperature using a liquid nitrogen cooled chuck. The derived defect densities for the CIGAS devices are shown in Figure 5.

A broad spectrum of defects was measured for all samples, but the peak defect density shifts in energy from about 0.48 eV above the valence band edge for the sample with the no Ga to about 0.21 eV above the valence band edge for the sample with about equal amounts of Ga and Al. The result for the highest Ga content sample is not shown due to the inability to extract a well defined escape frequency for this sample. The AS result (peak energy) for the sample with about equal amounts of Ga and Al is similar to that obtained by others for high Ga (no Al) devices, in which the peak defect density was found to be about 0.19 eV above the valence band edge.(5), and for low Al content CIAS devices, in which the peak defect density was found to be about 0.21eV above the valence band edge.(17) Similarly, the AS result (peak energy) for the sample with no Ga (CIAS) is similar to that obtained by others for wide-bandgap CIAS devices with bandgap in the range of 1.36 to 1.45 eV. (17)

Due to difficulty in obtaining an accurate value for the built-in potential from the capacitance-voltage measurement, the built-in potential was arbitrarily assumed to be 1 V for the derivation of the trap density. The assumption of same built-in potential was based on the similar bandgaps and zero-bias depletion widths among the devices. Consequently, the magnitudes of trap density are to be considered approximate. As such, the derived peak trap densities are found to be in the range of 6.0 – 12.0 x $10^{16}$ $cm^{-3}$ $eV^{-1}$ at room temperature (yellow open squares). Integrated trap densities have been correlated with Voc shortfall on low and high-bandgap CIGS devices.(4,18) The magnitude of trap densities measured for these devices would then correlate to significant

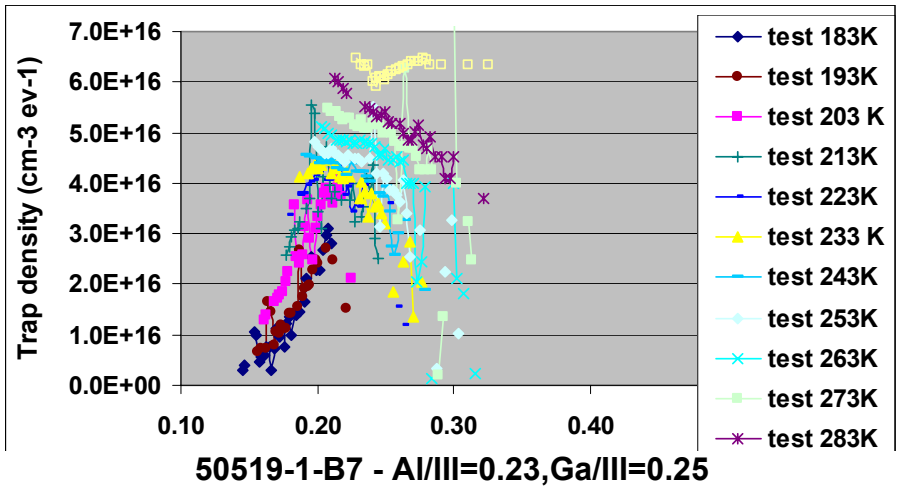


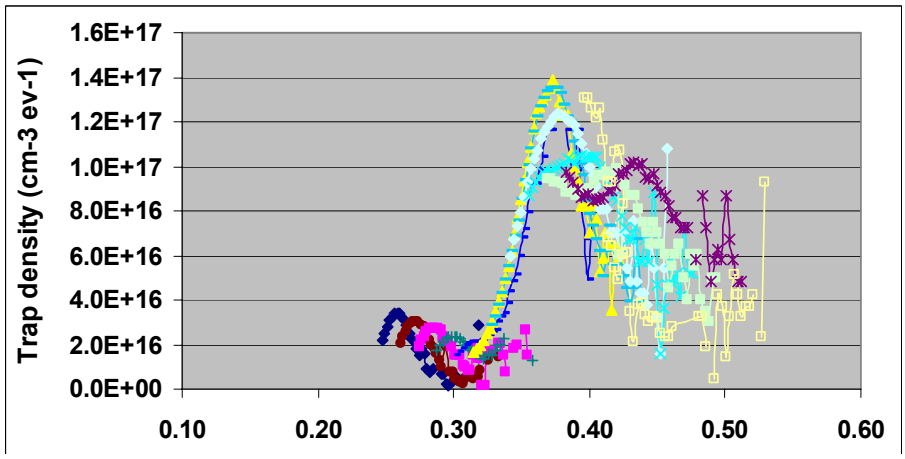


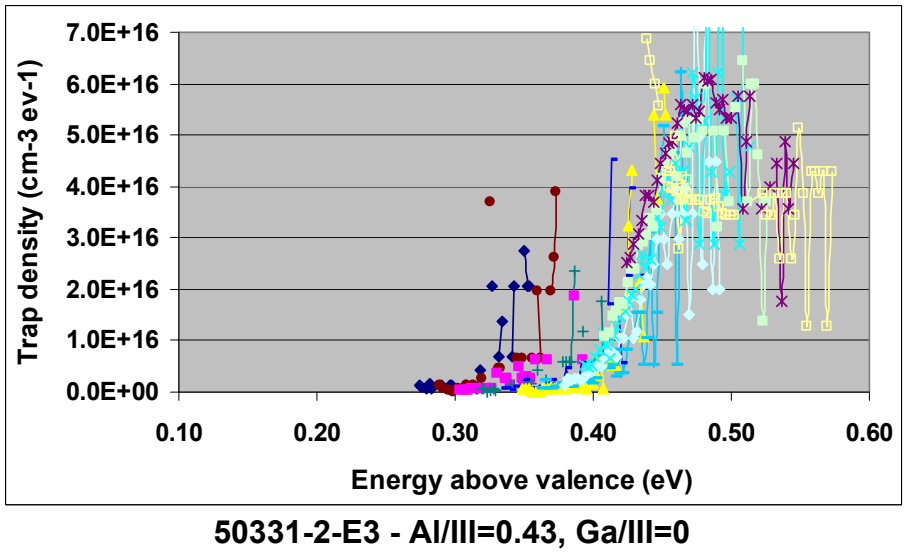


**Figure 5 - Admittance Spectroscopy from CIGAS devices with a bandgap in the narrow range of 1.45 – 1.48 eV, and as a function of Ga and Al content and temperature.**

voltage shortfall, and may be the dominant source for the generally low Voc values measured for these devices. Further characterization is needed to determine if other CIGAS devices with higher Voc's have lower defect densities; generally the higher Voc devices were the low Ga content devices.

The shift in the peak of defect densities indicates a change in the bulk defects as a function of composition (Ga and Al content), but with constant bandgap. However, it should be noted that the data could also be interpreted as defects at the CdS/CIGAS interface,(19) or a combination of bulk and interface states.

To determine if the dominant recombination mechanism is in the bulk or at the interface, the device Voc was measured versus temperature for two of the devices with different Ga and Al content: high Ga, low Al device, and high Al, low Ga device. The results are given in Figure 6.

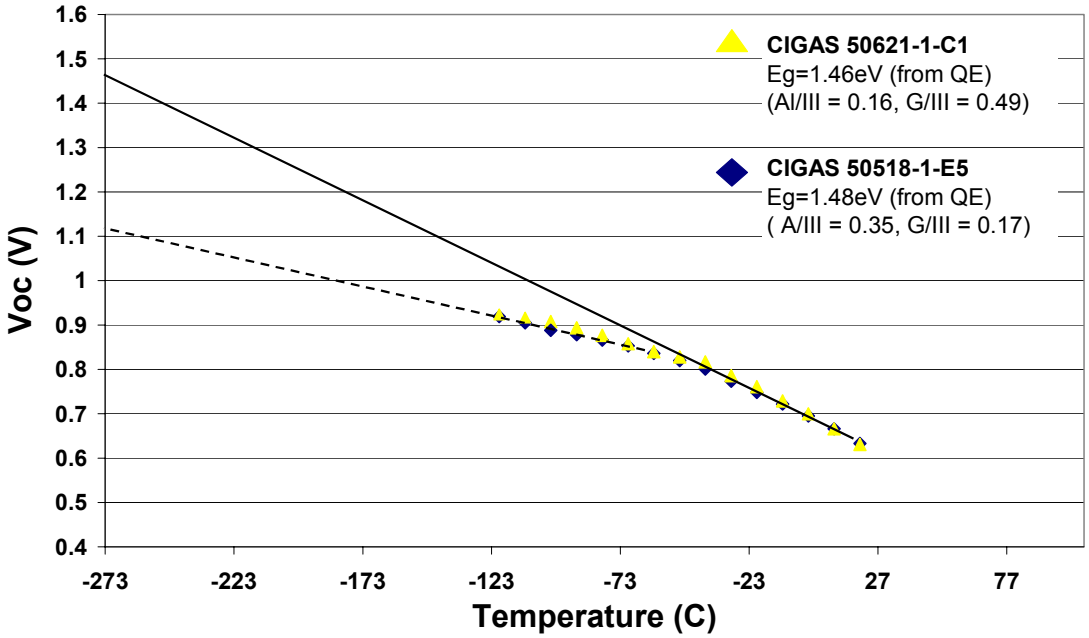


**Figure 6 – Voc versus temperature of a couple of samples with bandgap of about 1.46 – 1.48 eV, but one with high Al content (dark blue) and the other with high Ga content (yellow).**

In the figure it is shown that the high-temperature data extrapolates to about the room temperature bandgap, indicative of junction recombination.(4) while the low-temperature data extrapolates to a value much less than the bandgap. The low temperature results indicate that tunneling enhanced recombination and/or interface recombination begins to dominate in this temperature regime. (4,15) Assuming the presence of interface states at the CdS/CIGS heterointerface, then recent modeling has shown that interface recombination can also significantly reduce Voc when combined with a nearly flat conduction band line-up as predicted theoretically at the interface for the nominally 1.46 eV devices.(15)

## CIGAS Device Results on Novel High-Temperature and Flexible Silicone Substrates

When the CIGAS film compositions were in the target ranges from the wide-bandgap moving substrate deposition system, then subsequent depositions were attempted on both Mo coated flexible silicone substrates and TBC coated flexible silicone substrates. The silicone substrates also received an additional coating of NaF following the back contact deposition, and to provide a source of sodium to the CIGAS solar absorber. The device results for the devices with Mo back contact, and with TBCs are shown in Table 1 below, and compared to control devices on thick glass substrates. Unfortunately, these were not some of the better CIGAS devices, as indicated by the device performance. Nonetheless, the table shows that the devices on the lightweight and flexible substrates perform as well as devices on thick glass substrates.

**Table 1 – Summary of the device performance (Eff. and Voc) on lightweight and flexible silicone substrates and compared to devices with similar composition on glass substrates, and for both Mo and TBC back contact types.**

| Substrate | Back Contact | Device ID | Cu/III | Al/III | Ga/III | Best Eff. (%) | Best Voc (V) |
|---|---|---|---|---|---|---|---|
| Glass | Mo | 50524-2 | 0.65 | 0.33 | 0.2 | 3.0 | 0.495 |
| Glass | Mo | 50527-1 | 0.5 | 0.29 | 0.13 | 4.0 | 0.530 |
| Silicone | Mo | 50603-1 | 0.68 | 0.28 | 0.13 | 2.5 | 0.450 |
| Silicone | Mo | 50603-1 | 0.69 | 0.21 | 0.14 | 4.0 | 0.506 |
| Silicone | Mo | 50603-1 | 0.53 | 0.18 | 0.17 | 3.0 | 0.432 |
| Glass | TBC | 50615-2 | 0.71 | 0.14 | 0.49 | 2.5 | 0.580 |
| Glass | TBC | 50615-2 | 0.72 | 0.13 | 0.44 | 2.6 | 0.552 |
| Glass | TBC | 50615-2 | 0.65 | 0.16 | 0.36 | 3.6 | 0.574 |
| Glass | TBC | 50615-2 | 0.6 | 0.2 | 0.31 | 3.9 | 0.552 |
| Glass | TBC | 50616-1 | 0.74 | 0.14 | 0.5 | 2.2 | 0.474 |
| Glass | TBC | 50616-1 | 0.76 | 0.15 | 0.44 | 2.1 | 0.481 |
| Glass | TBC | 50616-1 | 0.75 | 0.16 | 0.38 | 2.2 | 0.472 |
| Silicone | TBC | 50624-1 | 0.59 | 0.14 | 0.47 | 2.5 | 0.513 |
| Silicone | TBC | 50624-1 | 0.67 | 0.11 | 0.44 | 4.1 | 0.606 |
| Silicone | TBC | 50624-1 | 0.69 | 0.13 | 0.4 | 4.0 | 0.587 |
| Silicone | TBC | 50624-1 | 0.57 | 0.2 | 0.26 | 3.9 | 0.555 |

## SUMMARY

Wide-bandgap CIGAS devices were fabricated with a wide range of bandgaps and Ga and Al content. Similar performance was generally observed over a wide range of CIGAS compositions at a given wide-bandgap despite the shift in the dominant defect distribution with Ga/Al content and indications of dominant junction recombination at room temperature. In certain subsections of the bandgap range, the CIGAS device results to date indicate potential for performance advantages with low-Ga content CIGAS solar absorbers. Finally, the development of high-temperature and highly transparent lightweight and flexible silicone substrates is promising, with demonstrated CIGAS device efficiencies that are comparable to glass substrates for both standard Mo back contacts and transparent back contacts.

## ACKNOWLEDGEMENTS

The results presented herein were obtained by work funded by a NASA SBIR Program, Contract No.: NNC05CA41C

## REFERENCES

[1] C. Clark, B. Zuckermandel, S. Enger, and D. Marcelli, “FITS, the Latest and Greatest Lightweight Solar Array for Space,” Proceeding of the 1st IECEC, Portsmouth, Va., (2003).

[2] S.G. Bailey, A.F. Hepp, and R.P. Raffaelle, “Thin Film Photovoltaics for Space Applications,” Proc. Of the 36th IECEC, pp. 235-238, (2001).

[3] M.A. Contreras, K. Ramanathan, J. Abushama, F. Hasoon, D. Young, B. Egaas and R. Noufi, “Diode Characteristics in State-of-the-art ZnO/CdS/$CuIn_{(1-x)}Ga_xSe_2$ Solar Cells”, *Progress in Photovoltaics: Research and Applications*, Vol. **13**(3), pp. 209-216, (2005).

[4] U. Rau, M. Schmidt, A. Jasenek, G. Hanna, H. Schock,”Electrical Characterization of $Cu(In,Ga)Se_2$ Thin-Film solar Cells and the Role of Defects for the Device Performance,” *Sol. Energy Mat. & Sol. Cells*, **67**, pp.137-143, (2001).

[5] J. Heath, J. Cohen, W. Shafarman, and D. Johnson, "Characterization of Deep Defects in $CuIn_{1-x}Ga_xSe_2$ (CIGS) Working Photovoltaic Devices," *Photovoltaics for the 21st Century II*, The Electrochemical Society, Inc., New Jersey, pp. 324-332, (2001).
[6] P. Paulson, M. Haimbodi, S. Marsillac, R. Birkmire and W. Shafarman,"$Cu(In_{1-x}Al_x)Se_2$ Thin Films and Solar Cells, *J. Appl. Phys*., **91**, pg. 10153, (2002).
[7] W. Shafarman et al., "Advances in $CuInSe_2$-based Solar Cells: From Fundamentals to Processing," NCPV and Solar Program Review Meeting, Denver, Co., pg. 525, (2003). The Comparison between CIGS and CIAS was presented during the conference.
[8] L.Woods, A.Kalla, D. Gonzalez, and R. Ribelin, "Wide-bandgap CIAS thin-film photovoltaics with transparent back contacts fo next generation single an multi-junction devices," *Mat. Sci. and Eng. B*, **116**, pp. 297-302 (2005).
[9] A. Rocket, "The Electronic Effects of Point Defects in $Cu(In_xGa_{1-x})Se_2$ Devices," Proc. of the 15th NCPV Photovoltaics Program Review, Edited by M. Al-Jassim et al., AIP 462, pp. 132-137. (1998).
[10] J. Heath, J. Cohen, W. Shafarman, D. Liao, and A. Rockett, "Effect of Ga Content on Defect States in $CuIn_{1-x}Ga_xSe_2$ Photovoltaic Devices," *Appl. Phys. Lett*., **80**(24), pp.1-3, (2002).
[11] Inferred from defect energy differences between Ga and In as given in: S. Wei, S. Zhang, and A. Zunger, *Appl. Phys. Lett.,* **72**(24), pgs. 3199-3201, (1998)
[12] C. P. Grant, Commun. In Partial Differential Equations, 18(3&4), pgs. 453-490 (1993).
[13] S. Marsillac, T. Wahiba, C. El Moctar, J. Bernede, A. Khelil," Evolution of the properties of $CuAlSe_2$ thin films with the oxygen content," *Sol. Energy Mat. & Sol. Cells*, **71**, pp.425-434, (2002).
[14] S. Zhang, S. Wei, and A. Zunger, "A phenomenological model for systematization and prediction of doping limits in II-VI and I-III-$VI_2$ compounds," *J. Appl. Phys*., **83**(6), pp3192-3196, (1998).
[15] M. Gloeckler and J.R. Sites, "Efficiency limitations for wide-bandgap chalcopyrite solar cells," E-MRS 2004 Spring Meeting.
[16] T. Walter, R. Herberholz, C. Muller and H.W. Schock, *J. Appl. Phys*, **80**(8), (1996)
[17] J. Health, J. Cohen, and W. Shafarman, "Defects in Copper Indium Aluminum Diselenide Films and their Impact on Photovoltaic Device Performance", Mat. Res. Soc. Symp. Proc. vol. 763, "Compound Semiconductor Photovoltaics," pp441-446, April (2003).
[18] I. Repins *et al*. (19 co-authors in total), "Comparison of Device Performance and Measured Transport Parameters in Widely-Varying Cu(In,Ga)(Se,S) Solar Cells," *Prog. Photovolt: Res. Appl.*, **13**, pp1-19, (2005).
[19] R. Herberholz, M. Igalson, and H. W. Schock, "Distinction between bulk and interface states in CuInSe2/CdS/ZnO by space charge spectroscopy," *J. Appl. Phys.*, **83**(1), pp318-325, (1998).